Hybrid Spectrum Sensing Test Statistic Based on the Gershgoring Theorem and on the Gini Index

Dayan Adionel Guimarães

National Institute of Telecommunications (*Instituto Nacional de Telecomunicações*) - Inatel, Santa Rita do Sapucaí, MG, Brazil

Abstract— The Gershgorin radii and centers ratio (GRCR) and the Gini index detector (GID) test statistics have been recently proposed as, blind, simple and robust solutions for centralized cooperative spectrum sensing under non-uniform and dynamical received signal and noise powers. In this paper, an hybridization of these test statistics is proposed, which is named hybrid GRCR-GID (HGG). It is demonstrated that the HGG harvests the advantages of the base detectors, attaining approximately the same performance of the GRCR in the absence of a dominant propagation path, and a little inferior performance with respect to the GID in the presence of dominant path. Moreover, the HGG is capable of outperforming the GRCR and the GID in some system configurations, maintaining robustness, low computational complexity, and the constant false alarm rate property.

Keywords— Cognitive radio, GID, GRCR, HGG, jamming detection, spectrum sensing.

I. Introduction

We are witnessing an unprecedented growth of telecommunication services, especially with regard to wireless communication systems. As a consequence, the radio-frequency (RF) spectrum has become an increasingly congested or even scarce communication resource in certain bands and regions, mainly due to the adoption of an spectrum allocation policy that assigns to primary systems, in a fixed fashion, the frequency portion associated to each service. The problem tends to worsen with the massification of the Internet of Things (IoT) and the deployment of the fifth generation (5G) of wireless communication networks, mainly due to the expected huge amount of terminals and the demand for higher bandwidths.

The concept of cognitive radio (CR) has emerged as a promising solution to the above problem [1], [2], accounting for the time-space-varying nature of the occupation state of certain frequency bands. It can take advantage of a dynamic spectrum access policy in which idle frequency bands due to underutilization can be opportunistically occupied by cognitive secondary user (SU) terminals. For this to occur, cognitive radios need to detect the presence of the primary user (PU) signals in the band of interest, a process called spectrum sensing [3], [4]. Moreover, the cognitive radios need to be agile enough to jump to the free band as soon as it is detected vacant, quickly moving out if the band is accessed again by any PU terminal.

The spectrum sensing capability is crucial not only to the dynamic spectrum access approach. In military communications, the presence of intentional (jamming) and unintentional

interference can be detected to drive frequency hopping operation or other countermeasure, aiming to maintain the desired level of communication quality and attain low probability of interception (LPI).

Spectrum sensing can be performed independently by each cognitive radio, or can resort to cooperation aiming at better performances. The former is subjected to problems that reduce the detection power, like multipath fading, shadowing and hidden terminals [3]. Cooperation improves the accuracy of the decisions on the occupation state of the sensed band compared to the non-cooperative sensing, owed to the spatial diversity promoted by the different geographic positions of the radios in cooperation.

In centralized cooperative sensing with data fusion, which is the focus of the present work, samples of the sensed signal, or quantities derived therefrom are transmitted to a fusion center (FC), where the final or global decision is made. This decision is then informed to the cognitive radios, who will compete for the band, if it is unoccupied, by means of some appropriate multiple access technique.

The metrics often used to assess the spectrum sensing performance are the probability of detection, P_d, and the probability of false alarm, P_{fa}. The former is the probability of deciding in favor of an occupied band, given that it is really occupied. The later is the probability of deciding in favor of an occupied band, given that it is in fact vacant. A high value of P_d is desired to reduce the interference caused by the secondary network to the primary network due to missed detections. On the other hand, a low value of P_{fa} is aimed at, so that more opportunistic transmissions can be made by the secondary network due to bands that are less frequently declared occupied when they are actually vacant.

A. Related research

The Gershgorin radii and centers ratio (GRCR) [5] and Gini index detector) (GID) [6] were recently proposed as solutions for centralized cooperative spectrum sensing with data fusion. In addition to having low computational complexity, they are robust against variations in the received signal and noise powers, they do not need knowledge about the characteristics of the sensed signal and about the noise power, meaning that they are completely blind detectors, and they have the property of constant false alarm rate (CFAR). Moreover, they are capable of outperforming most of the blind detectors available in the literature in a wide range of situations.

The GID has as its main characteristic the high performance when the sensed signal has a dominant propagation path component, either line-of-sight or specular. However, its performance is drastically affected in the absence of such

dominant path. The GRCR has no outstanding performance in the dominant path situation, but significantly outperforms the GID when path dominance does not exist.

Aiming at harvesting the desired attributes of the GRCR and the GID in different scenarios and system parameters, a linear combination of their test statistics has been proposed in [7] and [8]. The former applies to the detection of communication signals in general, whereas the later considers the detection of pulse radar signals under the sliding-window approach [9].

Other blind detectors deserve to be highlighted, for instance the Hadamard ratio (HR) [10], the volume-based detector number 1 (VD1) [11], and those based on the eigenvalues of the received signal covariance matrix [12], [13]: the generalized likelihood ratio test (GLRT), the arithmetic to geometric mean (AGM), and the maximum-to-minimum eigenvalue detection (MMED). Such detectors have similar computational complexities, but potentially different performances depending on the systemic parameters.

B. Contributions and structure of the paper

In this paper, the hybrid GRCR-GID (HGG) test statistic is devised. It is formed as a ratio of quantities in which the numerator comes from the GRCR test statistic and the denominator comes from the GID. It is demonstrated that the HGG achieves a combination of the best attributes of the GRCR and the GID, being capable of overcoming these basis detectors for some system parameters and scenarios. In most of the situations in which the performances are assessed under variations of system parameters, the performance of HGG unveils a compensating character: while one of the base detectors is penalized in performance for some parameter values and the other is improved, the HGG stays in between the performances achieved by the GRCR and the GID over practically the whole parameter variation ranges. Moreover, the HGG has low computational complexity, exhibits the constant false alarm rate property, and is robust against received signal and noise powers that might be nonuniform across the cognitive radios, as well as time-varying.

The remainder of the text is organized as follows: Section II describes the system model, presents the GRCR and the GID detectors, proposes the new HGG, and lists the state-of-the-art competing detectors chosen for comparison purposes. Section III is devoted to extensive numerical results and discussions. Section IV concludes the paper and gives directions for further related research.

II. SYSTEM MODEL

In this paper, a centralized cooperative spectrum sensing (CSS) with data fusion is adopted.

A. Signal model

The CSS is accomplished by means of m cognitive SUs, each one collecting n samples of the signal received from s primary transmitters during each sensing interval. At the FC, such samples form the matrix $\mathbf{Y} \in \mathbb{C}^{m \times n}$ given by

$$\mathbf{Y} = \mathbf{HX} + \mathbf{V}. \tag{1}$$

In this equation, the samples associated to the signals transmitted by the s PUs are arranged in the matrix $\mathbf{X} \in \mathbb{C}^{s \times n}$.

These samples are Gaussian distributed, with zero mean and variance dependent of the average signal-to-noise ratio (SNR) across the SUs. The Gaussian distribution is adopted due to the fact the it appropriately describes the envelope fluctuations of typical modulated and filtered communication signals [14].

The channel matrix $\mathbf{H} \in \mathbb{C}^{m \times s}$ in (1) is formed by elements h_{ij}, $i = 1, 2, \ldots, m$, $j = 1, 2, \ldots, s$, which represent the flat (frequency non-selective) sensing channel gains between the j-th PU and the i-th SU. These gains are assumed to be constant during the sensing interval and independent and identically distributed (i.i.d.) between consecutive sensing rounds, i.e., a slow block fading channel is assumed. This channel matrix is given by

$$\mathbf{H} = \mathbf{GA}, \tag{2}$$

where $\mathbf{A} \in \mathbb{C}^{m \times s}$ is the matrix whose elements $a_{ij} \sim \mathbb{CN}[\sqrt{K/(2K+2)}, 1/(K+1)]$, $i = 1, \ldots, m$, guarantee unitary second moment of the fading magnitude, and where K is the Rice factor [6], [15, pp. 211-219]. In a multipath fading channel, the Rice factor is the ratio between the power in the dominant multipath component and the power of the remaining ones. A larger K means a stronger line-of-sight (LoS) received signal. If $K = 0$, the Ricean fading specializes to the Rayleigh fading, which corresponds to no LoS. If $K \to \infty$, a pure additive white Gaussian noise (AWGN) channel results. For practical purposes, an almost-pure AWGN is observed if $K > 10$.

Following [5], the realistic scenario of possibly different received signal levels across the SUs is also considered herein; level differences can arise, for instance, due to different channel attenuations between the PU transmitters and the SU receivers. To take this fact into account, the matrix $\mathbf{G} \in \mathbb{R}^{m \times m}$ in (2) is a diagonal gain matrix given by $\mathbf{G} = \operatorname{diag}\left(\sqrt{\mathbf{p}/p_{\text{avg}}}\right)$, where $\mathbf{p} = [p_1, p_2, \ldots, p_m]^{\text{T}}$ is the vector with the received signal powers in each SU, and $p_{\text{avg}} = \frac{1}{m} \sum_{i=1}^{m} p_i$ is the average received signal power over all SUs.

Without loss of generality, the overall channel power gain is unitary, meaning that each PU transmits with a constant power given by p_{avg}/s. When nonuniform-dynamical received signal powers are considered, which means signal levels potentially different across the SUs and variable over time, it follows that $p_i \sim \mathcal{U}[0.05 p_{\text{avg}}, 1.95 p_{\text{avg}}]$ in each sensing round.

In the case of uniform noise, the matrix $\mathbf{V} \in \mathbb{C}^{m \times n}$ in (1) is formed by i.i.d. Gaussian noise samples with zero mean and variance σ^2, i.e $\mathbf{V} \sim \mathcal{NC}(0, \sigma^2 \mathbf{I})$, with $\mathbf{I}$ being the identity matrix of order m. In the case of nonuniform-dynamical noise, the elements of the i-th row of $\mathbf{V}$ have variance σ_i^2, $i = 1, \ldots, m$. Specifically, $\sigma_i^2 \sim \mathcal{U}[0.05 \sigma_{\text{avg}}^2, 1.95 \sigma_{\text{avg}}^2]$ during each sensing interval, where $\sigma_{\text{avg}}^2 = \frac{1}{m} \sum_{i=1}^{m} \sigma_i^2$ is the average noise variance across the SUs. Thus, the received SNR, in dB, averaged over all SUs is $\text{SNR} = 10 \log_{10}(p_{\text{avg}}/\sigma_{\text{avg}}^2)$.

B. GRCR and GID test statistics

At the FC, the received signal sample covariance matrix (SCM) is computed as

$$\mathbf{R} = \frac{1}{n} \mathbf{YY}^{\dagger}, \tag{3}$$

where $\dagger$ denotes the complex conjugate and transpose.

From [5], the GRCR test statistic, which is grounded on the Geshgoring circle theorem [16, p. 82], is given by

$$T_{\text{GRCR}} = \frac{\sum_{i=1}^{m} \sum_{j=1, j \neq i}^{m} |r_{ij}|}{\sum_{i=1}^{m} r_{ii}}, \qquad (4)$$

where r_{ij} is the element in the i-th row and j-th column of $\mathbf{R}$, for $i, j = 1, \ldots, m$.

The GID test statistic has been proposed in [6], and is grounded on the Gini index [17, p. 3400]. Apart from a constant factor that does not influence performance, this statistic is given by

$$T_{\text{GID}} = \frac{\sum_{i=1}^{m^2} |r_i|}{\sum_{i=1}^{m^2} \sum_{j=1}^{m^2} |r_i - r_j|}, \qquad (5)$$

where r_i is the i-th element of the vector $\mathbf{r}$ formed by stacking all columns of $\mathbf{R}$.

C. Proposed HGG test statistic

The proposed hybrid GRCR-GID test statistic is formed as a ratio of quantities in which the numerator comes from (4), and the denominator comes from (5), yielding

$$T_{\text{HGG}} = \frac{\sum_{i=1}^{m} \sum_{j=i, j \neq i}^{m} |r_{ij}|}{\sum_{i=1}^{m^2} \sum_{j=i}^{m^2} |r_i - r_j|}, \qquad (6)$$

where slight modifications with respect to (4) and (5) have been made in the lower limits of the rightmost summations to speed-up computation. This has been made owed to the complex-conjugate symmetry of $\mathbf{R}$, which produces repeated entries in these summations.

The global decision at the FC is made in favor of the presence of the PU signal in the sensed band (hypothesis $\mathcal{H}_1$) if $T_{\text{HGG}} > \lambda$, where λ is the decision threshold configured according to the desired performance. Otherwise, if $T_{\text{HGG}} \leq \lambda$, a vacant band (hypothesis $\mathcal{H}_0$) is declared.

It can be noticed from (4), (5) and (6) that the three detectors have roughly the same computational complexity, which is in fact dominated by the complexity associated to the computation of the sample covariance matrix given in (3), i.e., $\mathcal{O}(nm^2)$ [5], [6].

As stated in [5] and [6], the GRCR and the GID are the blind detectors with the lowest computational complexities known so far; the HGG is now added to these two, having the same computational cost growth in the big-$\mathcal{O}$ notation.

D. Competing detectors

As stated in Section I, the GLRT, the AGM, the MMED, the HR, and the VD1 test statistics form a list of recent blind detectors that are adopted in this article for comparisons with the GRCR, the GID and with the new HGG. The competing detectors have been chosen because they are representative of the state-of-the-art and have similar implementation complexities. According to [5], their complexities are $\mathcal{O}(nm^2) + \mathcal{O}(m^3)$, which is mainly owed to the computation of eigenvalues and determinants. Hence, it can be concluded that the complexity $\mathcal{O}(nm^2)$ of the HGG is considerably smaller.

The test statistics GLRT, AGM, MMED, HR and VD1 [10], [11], [12], [13], are, respectively

$$T_{\text{GLRT}} = \frac{\lambda_1}{\sum_{i=1}^{m} \lambda_i}, \qquad (7)$$

$$T_{\text{AGM}} = \frac{\frac{1}{m} \sum_{i=1}^{m} \lambda_i}{\left(\prod_{i=1}^{m} \lambda_i\right)^{\frac{1}{m}}}, \qquad (8)$$

$$T_{\text{MMED}} = \frac{\lambda_1}{\lambda_m}, \qquad (9)$$

$$T_{\text{HR}} = \frac{\det(\mathbf{R})}{\prod_{i=1}^{m} r_{ii}}, \qquad (10)$$

$$T_{\text{VD1}} = \log\left[\det(\mathbf{E}^{-1}\mathbf{R})\right]. \qquad (11)$$

In these expressions, $\lambda_1 \geq \lambda_2 \geq \cdots \geq \lambda_m$ are the eigenvalues of $\mathbf{R}$, $\det(\mathbf{R})$ is the determinant of $\mathbf{R}$, y_{ij} are the elements of $\mathbf{Y}$, r_{ij} are the elements of $\mathbf{R}$, and $\mathbf{E} = \text{diag}(\mathbf{d})$, in which $\text{diag}(\mathbf{d})$ is the diagonal matrix whose main diagonal is formed by the elements of the vector $\mathbf{d} = [d_1, d_2, \cdots, d_m]$, with $d_i = \|\mathbf{R}(i, :)\|_2$, being $\|\cdot\|_2$ the Euclidean norm.

III. Numerical Results

A. Verifying the constant false alarm rate (CFAR) property

The GRCR and the GID have the important property of CFAR, which guarantees that P_{fa} is not influenced by the noise power across the SUs' receivers. Hence, it is expected that the hybridization of these test statistics propagates their CFAR property to the HGG. In order to verify, Fig. 1 shows the empirical probability density functions (PDFs) of T_{HGG} under the hypotheses $\mathcal{H}_0$ and $\mathcal{H}_1$, for two different values of the noise variance σ_{avg}^2. Since the supports of the PDFs did not change with σ_{avg}^2, it is concluded that the proposed HGG detector exhibits the CFAR property.
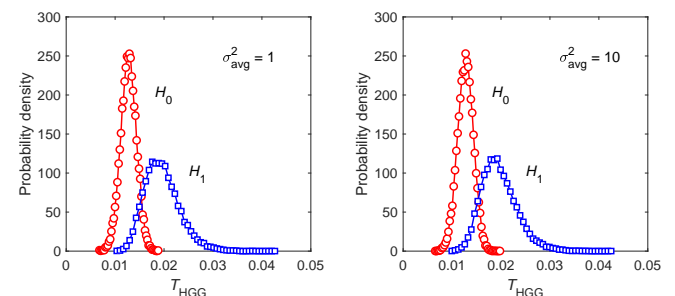

Fig. 1. Empirical PDFs of T_{HGG} under different noise variances, for SNR $= -8$ dB, $s = 1$, $m = 6$, $n = 50$, $K = 10$, and nonuniform-dynamical received signal and noise powers across the SUs.

B. Performance results

A typical graphical tool for analyzing the probabilities of detection (P_{d}) and false alarm (P_{fa}) simultaneously is the receiver operating characteristic (ROC) curve, which trades these probabilities as the decision threshold is varied. A condensed metric also often used is the area under the ROC curve (AUC). The worst and useless detector performance, which corresponds to a ROC curve with $P_{\text{d}} = P_{\text{fa}}$, gives AUC $= 0.5$. The optimum detector performance corresponds to a ROC curve attaining $P_{\text{d}} = 1$ and $P_{\text{fa}} = 0$, yielding AUC $= 1$. Hence, for a non-trivial detector, $0.5 < \text{AUC} \leq 1$.

In the following we present results of the AUC as a function of variations in all system parameters that are relevant to the spectrum sensing performance. Some ROC curves are also

given as closing results at the end of the section. All results were produced by computer simulations using the MATLAB software, version R2018a, from 30000 Monte Carlo events in which the received signal matrix $\mathbf{Y}$ was generated under the hypothesis $\mathcal{H}_1$ (to estimate P_d) and $\mathcal{H}_0$ (to estimate P_fa). The AUCs were computed using the built-in MATLAB function $-\mathtt{trapz}(P_\mathrm{fa}, P_\mathrm{d})$ from the corresponding ROC curves.

Fig. 2 presents AUCs versus the sensing channel Rice factor K, for $s = 1$ PU transmitter, $m = 6$ SU receivers, $n = 100$ samples, and average SNR $= -10$ dB, considering uniform (left) and nonuniform-dynamical (right) received signal and noise powers. Comparing the two graphs, one can notice that the detectors GRCR, GID, HGG, HR and VD1 are robust against nonuniform-dynamical signal and noise, since their performances exhibited small changes from the left to the right graph. Notice that the HGG unveiled practically unnoticeable change, meaning that it is more robust than the others. The eigenvalue-based detectors MMED, GLRT and AGM are clearly very sensitive to received signal and noise power variations, i.e., they are referred to as non-robust.
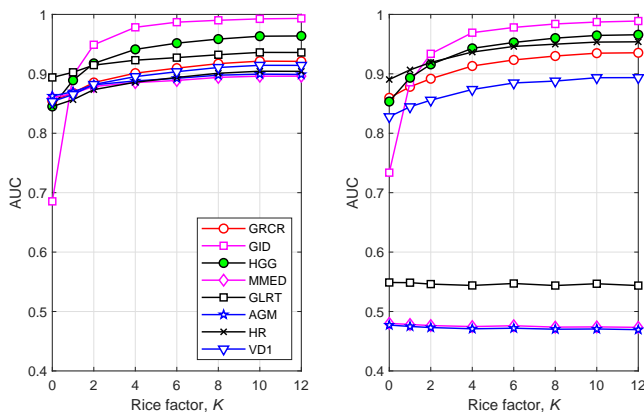

Fig. 2. AUC versus Rice factor (K), for $s = 1$, $m = 6$, $n = 100$ and SNR $= -10$ dB: uniform (left) and nonuniform-dynamical (right) signal and noise powers. Better viewed in color.

Fig. 2 also confirms the expected outcome of improved performances of the robust detectors as K increases. The improvement of the GID is quite distinct from the others, which is characteristic of its desired suitability to channels having some sort of propagation path dominance [6]. The HGG has produced an intermediate performance with respect to the GID and the GRCR, which is consistent with the motivation for hybridizing them to form the HGG. For the parameters at hand, the HGG is the second best detector from mild-to-high Rice factors, staying close to the top three detectors for any K.

Given that the robustness of the detectors can be determined from Fig. 2, and the fact that the nonuniform-dynamical signal and noise scenario is more realistic, the remaining AUCs shown hereafter assume only this situation.

Fig. 3 shows how the number of samples n affects the spectrum sensing performances. As expected, the increase of n yields performance improvements to the detectors in analysis, but in different amounts. The non-robust detectors (MMED, GLRT and AGM) are little influenced by n, and the GID lies in the middle for $K = 0$ because of its characteristic poor performance in this situation. It can also be noticed

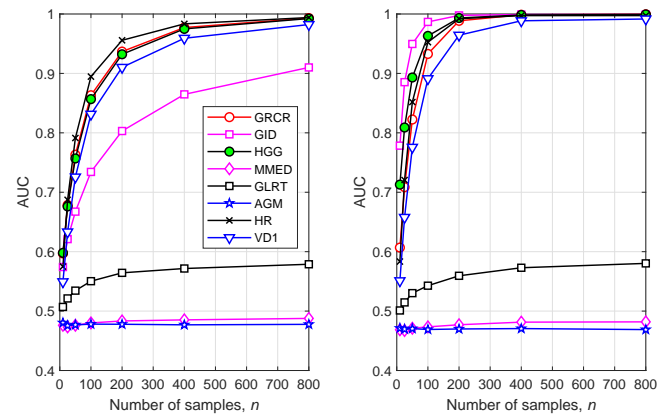that the proposed HGG lies among the top-three for any n, showing noticeable advantage for smaller numbers of samples.

Fig. 3. AUC versus number of samples (n), for $s = 1$, $m = 6$ and SNR $= -10$ dB: $K = 0$ (left), $K = 10$ (right). Better viewed in color.

The influence of the SNR is depicted in Fig. 4. In spite of the apparent uselessness of the non-robust detectors observed in the previous results, they indeed unveil attractive performance improvements with the SNR, above ≈ -12 dB, whereas the other detectors show monotonic performance improvements above -20 dB. When $K = 0$, the GID achieved a saturation-like behavior before the AUC approaches 1, meaning that the SNR wall [18] of this detector happens at lower SNR values. Again, the GID unveils top performance for any SNR when K is large. The HGG attains the second best performance among all competing detectors for any SNR, for the particular parameter setting adopted in this plot. The desired low sensitivity of the HGG to the Rice factor is again demonstrated, indeed combining the complementary sensitivities of the GID and the GRCR.
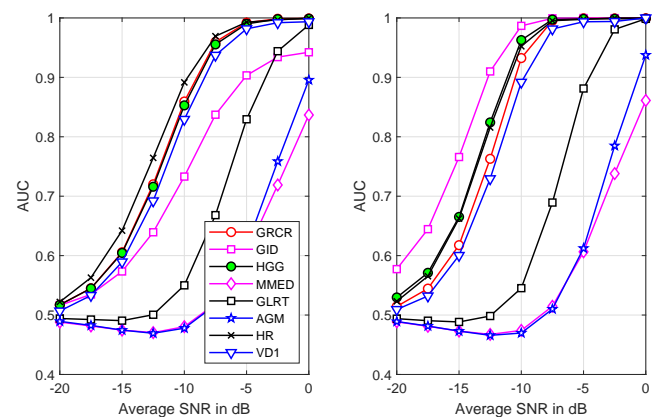

Fig. 4. AUC versus average SNR across the SUs, for $s = 1$, $m = 6$ and $n = 100$: $K = 0$ (left), $K = 10$ (right). Better viewed in color.

Fig. 5 reports the influence of the number of SUs, m, on the spectrum sensing performance. Mild improvements are verified for the non-robust detectors as m increases. The performance of the robust detectors improves as m is increased, but in a diminishing-return fashion. Once again, the poor performance of the GID when $K = 0$ is observed, while it attains top performance for any m in the situation of

large K. The HGG lies near to the second rank for any K (as already observed in Fig. 2), and any m.
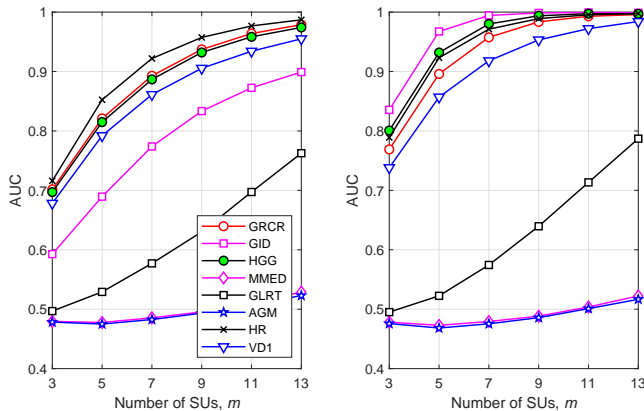

Fig. 5. AUC versus number of SUs (m), for $s = 1$, $n = 100$ and SNR $= -10$ dB: $K = 0$ (left), $K = 10$ (right). Better viewed in color.

The performance variations with the number of PU transmitters, s, are depicted in Fig. 6. The non-robust detectors (MMED, GLRT and AGM) again unveil poor performances due to the low SNR regime (see Fig. 4), and are little affected by the value of s for any K. When K is high, all detectors practically do not exhibit performance variations with s. When $K = 0$, the performances of the robust detectors (GRCR, GID, HGG, HR and VD1) are penalized as s is increased, but in different amounts. The HGG lies near to the second rank position for any s.
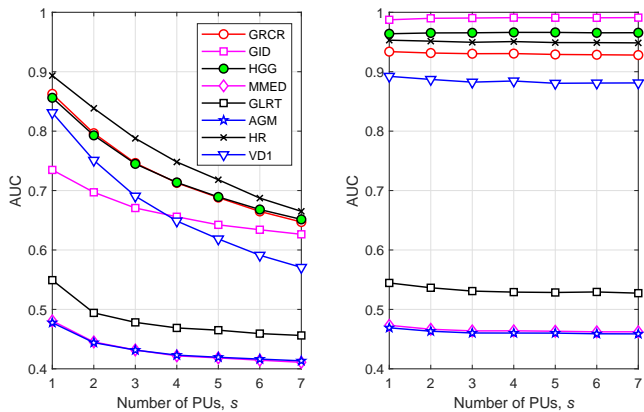

Fig. 6. AUC versus number of PUs (s), for $m = 6$, $n = 100$ and SNR $= -10$ dB: $K = 0$ (left), $K = 10$ (right). Better viewed in color.

In all performance results presented up to this point, it is worth observing the excellent performance of the HR detector, being always among the top three for any system parameterization, in many situations occupying in the top rank position. Nonetheless, one must be aware of the high computational complexity of this detector (compared with the HGG), as stated in the end of Subsection II-D.

Finally, one should bear in mind that, in practice, there are situations in which we are forced to adopt specific system parameters, for instance when the degree of freedom is reduced by the intrinsic and almost-always present systemic restrictions. However, it is not unlikely to have full flexibility to freely set most of the parameters, if not all. Hence,

the results presented in this section can be used to find system configurations and scenarios that yield the intended performance of any of the addressed detectors. Based on these arguments, closing results are shown in Figs. 7 and 8 in terms of ROC curves, where a set of parameters is unfavorable (Fig. 7) to the HGG detector, and another one is favorable (Fig. 8).
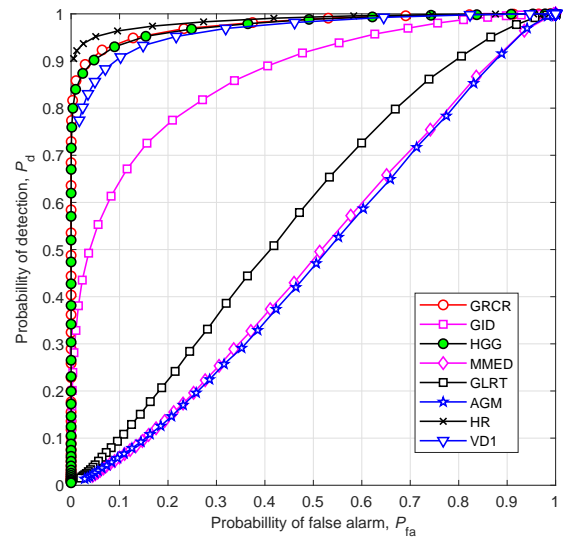

Fig. 7. ROC curves considering an unfavorable system parameter setting: $K = 0$, $n = 400$, SNR $= -10$ dB, $m = 6$, $s = 1$, and nonuniform-dynamical signal and noise levels. Better viewed in color.

The unfavorable parameters are $K = 0$ with nonuniform-dynamical signal and noise powers (given the worse performance of the HGG shown in Fig. 2 in this situation); $n = 400$ (practically no performance gain of the HGG with respect to the GRCR, as shown in Fig. 3 for $K = 0$); SNR $= -10$ dB (due to its slightly worse performance with respect to the GRCR, as shown in Fig. 4 for $K = 0$); $m = 6$ (any value of m can be chosen, since the relative performances of the HGG with respect to the GRCR and the GID practically do not change with m); $s = 1$ (due to its slightly worse performance with respect to the GRCR, as identified in Fig. 6 for $K = 0$).

The parameters favorable to the HGG (somewhat favorable to the other detectors as well) are $K = 10$ with uniform signal and noise powers (given its attractive performances shown in Fig. 2); $n = 100$ (as shown in Fig. 3 for $K = 10$, smaller numbers of samples are favorable to the HGG); SNR $= -10$ dB (due to the second best performance of the HGG, as shown in Fig. 4 for $K = 10$); $m = 6$ (for the same reason given to justify the previous set); $s = 4$ (since practically the same performance is achieve for any s, as identified in Fig. 6 for $K = 10$).

Fig. 7 unveils that even under unfavorable parameterization the HGG is capable of performing close to the best detector in this case, which is the HR. It can be also noticed that, in this situation, the performance of the HGG is very close to the GRCR, and away better than the GID.

In the favorable scenario, from which the other detectors also benefit, the GID shows up in the top position in Fig. 8, which is credited to the high Rice factor. The HGG comes in the second place, considerably far away from the remaining detectors.
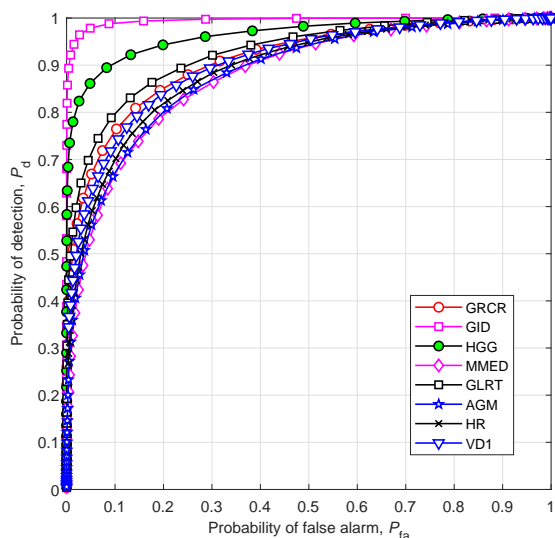
Fig. 8. ROC curves considering a favorable system parameter setting: $K = 10$, $n = 100$, SNR $= -10$ dB, $m = 6$, $s = 4$, and uniform signal and noise levels. Better viewed in color.

IV. Conclusions

An hybridization of the test statistics GRCR and GID has been proposed. The resultant blind detector was named hybrid GRCR-GID (HGG). It has been demonstrated that the HGG combines, as desired, the advantages of the base detectors, attaining approximately the same performance of the GRCR in the absence of a dominant propagation path, and a little inferior performance with respect to the GID in the presence of dominant path. The advantage of the HGG over the GID in the absence of a dominant path is considerably large for any system parameterization. Additionally, the HGG is capable of outperforming the GRCR in some system configurations, maintaining robustness against nonuniform-dynamical signal and noise levels, with very low computational complexity and compliant with the constant false alarm rate property.

The GRCR and the GID test statistics have been also combined in [7] and [8] in terms of a weighted sum. The resultant detector was named weighted GRCR-GID (WGG). Comparing the results presented here with those reported in [7], it can be seen that the HGG and the WGG achieve approximated performances, but the HGG has lower computational complexity, since, in the case of the WGG, the test statistics of the GRCR and the GID must be both computed in order to be subsequently combined linearly. Furthermore, the WGG needs the computation of the weights applied to the linear combination, a process that has been accomplished empirically in [7] and [8].

As opportunities for further related research, one could think about other combinations of the GRCR and the GID test statistics, or even between other test statistics that have the same root, which is the case, for example, of the eigenvalue based detectors. The sensing channel model could be also improved by adding shadowing effects and frequency selectivity. Another possibility would be to add impairments to the transmissions of the samples from the SUs to the FC, like quantization errors caused by the digitization of the sample values, channel-induced bit errors.

References

[1] J. Mitola III and G. Q. Maguire Jr., "Cognitive radio: making software radios more personal," vol. 6, no. 4, pp. 13–18, Aug. 1999.

[2] L. Zhang, M. Xiao, G. Wu, M. Alam, Y. Liang, and S. Li, "A survey of advanced techniques for spectrum sharing in 5G networks," *IEEE Wireless Communications*, vol. 24, no. 5, pp. 44–51, October 2017.

[3] I. F. Akyildiz, B. F. Lo, and R. Balakrishnan, "Cooperative spectrum sensing in cognitive radio networks: A survey," *Elsevier Physical Comm.*, vol. 4, pp. 40–62, Mar. 2011.

[4] Y. Arjoune and N. Kaabouch, "A comprehensive survey on spectrum sensing in cognitive radio networks: Recent advances, new challenges, and future research directions," *Sensors*, vol. 19, no. 1, 2019. [Online]. Available: http://www.mdpi.com/1424-8220/19/1/126

[5] D. A. Guimarães, "Robust test statistic for cooperative spectrum sensing based on the Gerschgorin circle theorem," *IEEE Access*, vol. 6, pp. 2445–2456, 2018, doi: 10.1109/ACCESS.2017.2783443. [Online]. Available: https://ieeexplore.ieee.org/abstract/document/8207427

[6] D. A. Guimarães, "Gini index inspired robust detector for spectrum sensing over Ricean channels," *Electronics Letters*, November 2018. [Online]. Available: https://digital-library.theiet.org/content/journals/10.1049/el.2018.7375

[7] D. A. Guimarães, "Linear combination of test statistics for cooperative spectrum sensing (original title in Portuguese: *combinação linear de estatísticas de teste para sensoriamento espectral cooperativo*)," in *XXXVII Brazilian Telecommunications Symposium, SBrT'19*, Sep 2019.

[8] D. A. Guimarães and C. H. Lim, "Hybrid sliding-window based detector for spectrum sensing in radar bands," *Journal of Communication and Information Systems, JCIS*, vol. 34, no. 1, pp. 192–200, July 2019, doi: 10.14209/jcis.2019.20. [Online]. Available: https://jcis.sbrt.org.br/jcis/article/view/668

[9] D. A. Guimarães and C. H. Lim, "Sliding-window-based detection for spectrum sensing in radar bands," *IEEE Communications Letters*, vol. 22, no. 7, pp. 1418–1421, July 2018.

[10] D. Ramirez, G. Vazquez-Vilar, R. Lopez-Valcarce, J. Via, and I. Santamaria, "Detection of rank-p signals in cognitive radio networks with uncalibrated multiple antennas," vol. 59, no. 8, pp. 3764–3774, Aug. 2011.

[11] L. Huang, H. So, and C. Qian, "Volume-based method for spectrum sensing," *Digital Signal Processing*, vol. 28, pp. 48–56, 2014.

[12] B. Nadler, F. Penna, and R. Garello, "Performance of eigenvalue-based signal detectors with known and unknown noise level," in *IEEE Int. Conf. Communications*, Jun. 2011, pp. 1–5.

[13] R. Zhang, T. J. Lim, Y. C. Liang, and Y. Zeng, "Multi-antenna based spectrum sensing for cognitive radios: A GLRT approach," *IEEE Transactions on Communications*, vol. 58, no. 1, pp. 84–88, Jan. 2010.

[14] B. Nadler, F. Penna, and R. Garello, "Performance of eigenvalue-based signal detectors with known and unknown noise level," in *IEEE Int. Conf. Communications*, Jun. 2011, pp. 1–5.

[15] D. A. Guimarães, *Digital Transmission: A Simulation-Aided Introduction with VisSim/Comm*, ser. Signals and Communication Technology. Springer-Verlag, 2009.

[16] J. W. Demmel, *Applied Numerical Linear Algebra*. Philadelphia, PA, USA: Society for Industrial and Applied Mathematics, 1997.

[17] S. Kotz, N. Balakrishnan, C. B. Read, and B. Vidakovic, *Encyclopedia of Statistical Sciences*, 2nd ed. Wiley-Interscience, 2006.

[18] R. Tandra and A. Sahai, "SNR walls for signal detection," *IEEE Journal of Selected Topics in Signal Processing*, vol. 2, no. 1, pp. 4–17, Feb 2008.